

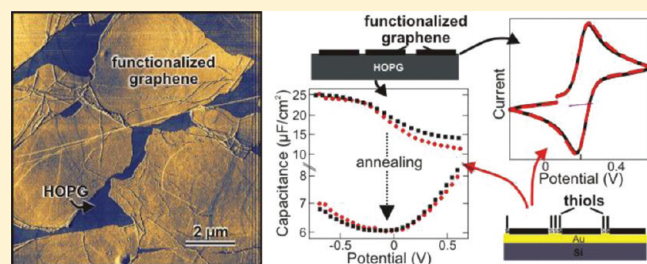
Intrinsic Capacitance and Redox Activity of Functionalized Graphene Sheets

Michael A. Pope, Christian Punckt, and Ilhan A. Aksay*

Department of Chemical and Biological Engineering, Princeton University, Princeton, New Jersey 08544, United States

Supporting Information

ABSTRACT: We present a general method for characterizing the intrinsic electrochemical properties of graphene sheets, such as the specific double-layer capacitance, in the absence of porosity-related artifacts and uncertainties. By assembling densely tiled monolayers of electrically insulating or conductive functionalized graphene sheets onto electrode substrates (gold and highly oriented pyrolytic graphite), we demonstrate our ability to isolate their intrinsic electrochemical response in terms of surface-specific double-layer capacitance and redox behavior. Using this system, the electrochemical properties of various types of graphene can be directly compared without the need to take into account changes in electrode morphology and electrolyte accessibility arising because of varying material properties.



1. INTRODUCTION

Functionalized graphene sheets (FGSs) produced by the exfoliation and reduction of graphite oxide^{1,2} (GO) exhibit clear advantages in electrochemical applications involving sensing, electrocatalysis, and energy storage compared with other nanoscale carbonaceous materials such as carbon black (CB) and carbon nanotubes (CNTs).^{3–7} The unique electrochemical properties of FGSs are attributed to their large number density of functional groups (epoxy, hydroxyl, and carboxylic acid groups) and lattice defects as well as their large specific surface area of theoretically 2630 m²/g.^{1,2} The experimentally accessible surface area depends largely on the state of aggregation. The unconsolidated material has been measured to have a surface area as large as 1850 m²/g, indicating that the material indeed exists in a predominately single sheet form when dispersed as a colloidal suspension.² This has been confirmed with atomic force microscopy (AFM) studies.¹ Aggregates of FGSs exhibit a smaller surface area typically ranging from 300 to 700 m²/g.^{1,2,8}

The FGSs we work with are prepared by thermal exfoliation and reduction,^{1,2} whereas they can also be prepared by the chemical reduction of graphene oxide.⁹ Both processes yield FGSs free of metal contaminants that otherwise could have a significant impact on the electrochemical response of the material.^{10,11} For reasons that are currently not well understood, the carbon-to-oxygen (C/O) ratio of FGSs prepared by the chemical reduction of graphene oxide typically does not exceed 14,^{12,13} whereas FGSs produced by the rapid thermal expansion of GO can reach C/O ratios exceeding 300.^{8,14,15} Thermal exfoliation combined with thermal post-treatment provides a means for tailoring the degree of functionalization and defectiveness of FGSs for electrochemical studies.^{8,14,15} The C/O ratio of FGSs therefore provides an estimate for the degree of

reduction of the material,^{8,12} that is, for the number density of oxygen-containing functional groups,^{5,6,24} and we designate the specific C/O ratio x as FGS _{x} . The most oxidized form of FGSs, known as graphene oxide, has a C/O ratio of ~ 2 (thus, referred to as FGS₂) and is electrically insulating.

A major difficulty in measuring the intrinsic electrochemical properties of FGSs is the lack of a well-defined electrode system: A meaningful interpretation of electrochemical measurements relies on the precise knowledge of the electrochemically active surface area, electrode geometry, and porosity.^{8,16} These properties are difficult to control with electrode materials such as FGSs or CNTs because preparing electrodes from these materials typically results in porous films when fabricated by methods such as drop-casting or filtration of dispersed suspensions or slurries.⁸ For FGSs, the surface area of dried electrode films made from suspensions or slurries varies between 44 and 700 m²/g, depending on the type of FGSs and on the processing conditions.^{8,15,17,18} The inability to control the accessible surface area and the porosity of the FGS aggregates when they are produced as thick films leads to difficulties in measuring the intrinsic electrochemical properties of the material such as the double-layer capacitance (a key parameter for energy storage applications) or the electron transfer rates and redox potentials important for electrocatalysis and sensing.^{8,19}

In a recent case study on the role of process-specific aggregation, we demonstrated that the evaporative coating of substrates with FGS suspensions in different solvents causes the dried films of FGSs to exhibit largely different porosities.⁸ The film porosity

Received: July 18, 2011

Revised: August 31, 2011

Published: September 06, 2011

was correlated with changes in the oxidation overpotential for nicotinamide adenine dinucleotide (NADH), which severely complicated a direct comparison between different types of FGSs and also prevented a direct observation of the intrinsic electrocatalytic capabilities of FGSs. Similarly, Menshkykau and Compton showed in recent theoretical studies that electrode roughness and porosity can lead to the observation of effective electrocatalytic behavior of an electrode.¹⁶

The measurement of the surface specific double-layer capacitance (C_{dl}) of an electrode, an important metric for comparing the charge storage capabilities of materials used for electrochemical double-layer capacitors (EDLCs), is severely affected by electrode morphology. For example, Goh and Pumera have shown that the mass specific capacitance of multisheet graphene nanoribbons is larger than single sheets.²⁰ This was attributed to overlap between single sheets, especially at edge-plane sites that are known to have higher capacitance than the basal-plane.²¹ Brownson and Banks²² showed that processing of electrodes with or without surfactant and binder can also significantly impact the measured capacitance of porous graphene-based electrodes. Furthermore, in a porous system, the measurement of a material's intrinsic C_{dl} involves estimating the ion accessible surface areas by gas adsorption measurements. However, it is still not well understood which pore sizes contribute to double-layer charging,²³ and it has also been claimed that pore size may have an effect on the measured C_{dl} of an electrode²⁴ and therefore may introduce substantial errors in the estimation of this important parameter.

To circumvent morphology-related measurement artifacts, fundamental studies of double-layer charging or other electrochemical properties are, whenever possible, carried out on well-polished flat electrodes. For instance, the intrinsic capacitance of carbon surfaces such as glassy carbon,²¹ boron-doped diamond,²⁵ and single-crystal graphite electrodes^{21,26} has been measured with this approach. More recently, microfabrication techniques have been employed to isolate electrodes of single pristine graphene sheets ranging in size from tens of micrometers to millimeters in diameter produced by both mechanical exfoliation of graphite ("Scotch-tape" method)^{27,28} and by chemical vapor deposition (CVD)²⁸ to measure their electrochemical properties. These studies suggested that pristine graphene behaves similarly to the basal-plane of highly oriented pyrolytic graphite (HOPG), which has a low C_{dl} and slow electron transfer kinetics.^{26,29}

FGSs, however, are expected to exhibit a rich and diverse electrochemistry due to the presence of lattice defects and functional groups. To support this conjecture, we need to develop a suitable method for measuring the intrinsic electrochemical properties of such a material. The micropatterning techniques developed for pristine graphene would be difficult to apply to FGSs because the majority of FGSs are $<1 \mu\text{m}$ in size.^{1,2} Contacting such submicrometer sheets and masking these contacts would require tedious nanopatterning techniques. Also, electrical contacts cover the edges of graphene sheets and limit electrochemical measurements to the basal-plane of graphene only. It is also likely that patterning in general may alter the electrochemical properties of FGSs, and the performance of individual sheets may not be representative of the unprocessed material.

To avoid these problems, the approach taken in our work involves the dense packing of a large ensemble of single sheets lying flat on a planar electrode substrate. A convenient and controllable method for preparing such a monolayer is to first assemble FGSs at the air–water interface in a Langmuir–Blodgett (LB) trough. This has been demonstrated previously both for FGS₂³⁰

and for pristine graphene produced by the direct exfoliation of expanded graphite.³¹ We use a modified version of these approaches in this study to coat electrode surfaces with FGS₂ and other types of FGSs. Basal-plane HOPG and passivated gold are used as substrates for the monolayer coatings and to demonstrate our ability to measure the intrinsic C_{dl} and redox capabilities of FGSs with minimal contribution from the underlying substrates.

2. EXPERIMENTAL SECTION

Production of FGSs. FGSs with different C/O ratios were prepared for this study by systematically varying the reduction and annealing treatments. To synthesize FGS₂ used for LB coatings, a modified Hummer's method³² was carried out according to the procedure of Cote et al.³⁰ While continuously stirring in an ice bath, a slurry of 0.5 g of graphite, 0.5 g of NaNO₃, and 23 mL of H₂SO₄ was prepared. After the addition of 3 g of KMnO₄, the slurry was heated to 35 °C and stirred at that temperature for 1 h. Subsequently, we added 400 mL of water and stirred the resulting suspension for 30 min while raising the reaction temperature to ~90 °C. The suspension was then diluted with another 100 mL of water, followed by 3 mL of H₂O₂ (30%). Subsequently, centrifugation was used to separate FGS₂ from the soluble components of the reaction mixture and also to select for large sheets that float at the air–water interface more easily.^{30,33}

Thermally reduced FGSs prepared by the rapid thermal expansion of GO (GO preparation proprietary) were provided by Vorbeck Materials Corporation (batch BK86X) and had a C/O ratio of 13. For measurements on FGSs with C/O ratios >13 , we reduced this material further by heat-treatment in a nitrogen atmosphere at 1500 °C for 2 h using a resistively heated graphite furnace (Astro-1000, Thermal Technologies).

FGS Characterization. The C/O ratio of FGSs was determined by combustion analysis (Atlantic Microlabs, GA). Before and after heat treatment, FGS powder was analyzed by X-ray diffraction (XRD) using a Miniflex II (Rigaku Americas, Cu $K\alpha$ radiation) and Raman spectroscopy (Kaiser Optics, $\lambda = 532 \text{ nm}$). The nitrogen accessible surface area was determined according to the Brunauer, Emmett, and Teller (BET)³⁴ method using a Gemini V unit (Micromeritics Instruments).

Preparation of Monolayer Electrodes. Aqueous suspensions of FGS₂ were mixed with methanol at a volume ratio of 1:5 water to methanol.³⁰ FGSs with C/O ratios of 13 and above were suspended in residue-free 1,2-dichloroethane (DCE) at a concentration of 5 mg per 15 mL, and the resulting suspensions were tip-ultrasonicated in an ice bath for 30 min at 60% amplitude (150 W, Branson Ultrasonics). Aggregates were removed by centrifugation at 3000 rpm for 60 min, and the supernatant was diluted 3:1 with pure DCE.

The suspensions were spread out on the air–water interface of an LB trough (Nima Technology, maximum area of 280 cm²) using a syringe pump set at a flow rate of 0.1 mL/min. A sufficient coverage of FGS₂ was attained after the addition of only 1 mL of suspension, whereas the other FGS suspensions required 3–5 mL. The FGS₂ coverage was observed with a Brewster angle microscope (BAM, BAM2plus, Nanofilm Technologie GmbH), and the surface tension was monitored using a Wilhelmy plate cut from filter paper. LB films of reduced FGSs could be observed as a faint dark film with the naked eye, and thus the BAM was unnecessary. Movable Teflon barriers were used to adjust the surface pressure at a speed of 30 cm²/min.

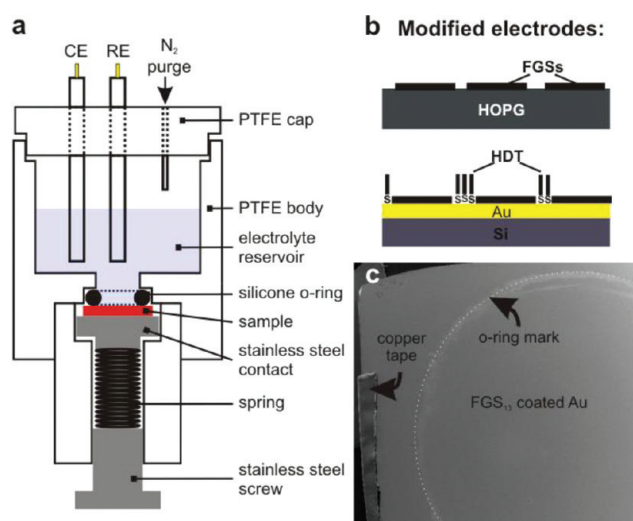


Figure 1. Overview of experimental approach. (a) Schematic of electrochemical cell where electrodes are spring-loaded against a silicon O-ring to define the electrochemically active surface area. (b) Schematic of monolayer electrodes on HOPG and silicon-coated with Au. (c) Scanning electron micrograph of a continuous FGS monolayer film on gold after electrochemical cycling. The O-ring removes some of the FGSs allowing us to estimate the active surface area (indicated by the dashed white ring).

The LB films were transferred to various substrates by the horizontal deposition method.³⁵ Dip coating was not performed because the adhesion of FGS films to the HOPG surface was insufficient. Multiple substrates were placed in the cleaned deionized water subphase in the absence of the LB film. Once the LB film was under compression, it was lowered onto the various surfaces by slowly pumping water out of the trough. Coated samples were air-dried for 15 min and then transferred to an Ar-filled glovebox and placed on a hot plate at 80 °C to dry overnight.

Electrochemical Setup. A homemade electrochemical cell was designed as shown schematically in Figure 1a to hold block-type electrodes of HOPG and gold evaporated onto pieces of silicon wafer. This design is a slightly modified version of the electrode holder described by Randin and Yeager²⁶ and later modified by Compton's group.³⁶ The electrodes are spring-loaded against a silicone O-ring that is used to isolate the electrochemically active surface area. In this design, the electrolyte reservoir is built into the electrode holder, and the electrode faces upward, which prevents any gases (from purging or electrolysis) to accumulate in the divot formed by the holder. The screw-on Teflon lid features ports for a Pt counter electrode, a double-junction Ag/AgCl reference electrode (inner and outer compartment filled with 1 M KCl and 0.5 M NaF, respectively) and a Teflon hose for nitrogen purging. All potentials are reported versus the Ag/AgCl reference electrode (1 M). (A double-junction reference electrode was used since trace amounts of chloride complex with gold at high potentials, which was found to significantly alter the electrochemical response of the gold electrodes used.)

As shown in Figure 1b, we used either HOPG blocks or gold films evaporated onto silicon wafers as substrates for the FGS films. The gold substrates were prepared by evaporating a 10 nm adhesion layer of Ti, followed by 50 nm of a Pt diffusion barrier and a final 300 nm gold coating using an e-beam evaporator

(Angstrom Engineering). Electrodes were cut into 1 cm × 1 cm pieces and annealed for 4 s in a H₂ flame to clean the surface and to create large gold domains with near atomic smoothness.³⁷ HOPG working electrodes (Grade 2) were obtained from Structure Probe. Prior to each experiment, the top layer was peeled off with a piece of adhesive tape to expose a fresh basal-plane HOPG surface. (Below, the term HOPG is used to denote the basal-plane of HOPG.) Gold and HOPG cleaning procedures were performed within 15 min prior to LB coating or electrochemical measurements to minimize the adsorption of contaminants from the environment. The gold surfaces were modified with hexadecanethiol (HDT) or 16-mercaptohexadecanoic acid (MHDA) by soaking them in 1 mM solutions of HDT or MHDA in ethanol for at least 4 h.

Characterization of Electrodes. Electrodes were characterized by scanning electron microscopy (SEM, VEGA1, Tescan USA) at 20 kV acceleration voltage using the secondary electron detector. The O-ring seal of the cell leaves a mark on the electrode surfaces (Figure 1c), which we used to determine the geometric surface area of the part of the electrode that was exposed to the electrolyte. The relative coverage A_{rel} of the electrodes with FGSs was determined by SEM image analysis (MatLab): Images were taken at five different randomly chosen locations within an area of 1 cm². Morphology and height of various FGSs on the gold and HOPG surfaces were determined using tapping-mode and contact-mode AFM, carried out with a MultiMode/Digital Nanoscope IIIa system (Veeco Instruments) using RTESP and NPS-type tips to confirm if single-sheet monolayers indeed formed.

Cyclic voltammetry and electrochemical impedance spectroscopy (EIS) were performed using a computer-controlled digital potentiostat (VSP, Bio-Logic USA). Aqueous electrolytes of 0.5 M NaF or 10 mM HClO₄ were used as supporting electrolytes because they are not electrochemically active on gold or HOPG and minimize specific adsorption.³⁸ A 5 mM solution of potassium ferrocyanide was used as a redox probe with 0.5 M NaF as the supporting electrolyte. The solution resistance was measured before cyclic voltammetry tests and compensated during the measurements.

3. RESULTS AND DISCUSSION

To prove the validity of the results obtained with our setup, we first present the capacitance and redox activity of highly reduced and annealed FGSs, which we expect to be similar to those of HOPG and pristine graphene and which can be compared with data published in the literature.^{26,27} We then analyze the other extreme, fully oxidized graphene, FGS₂, which is expected to act as a blocking layer because it is an insulator. After confirming that measurements carried out on these reference systems give the expected results on both gold and HOPG substrates, we demonstrate the vastly different properties of FGSs with intermediate C/O ratio.

Reduction and Annealing of FGS Powder. FGS₁₃ had a specific surface area of 580 m²/g, and there was no noticeable graphite or GO peak in its XRD spectrum (Figure 2a), which is indicative of completely exfoliated FGSs.^{1,2} When the 1500 °C heat treatment was applied to FGS₁₃, the C/O ratio increased to 385, the surface area decreased to 380 m²/g, and a broad graphite d_{0002} peak became apparent in the XRD profile. The increase in the C/O ratio from 13 to 385 indicates that many of the oxygen-containing functional groups were removed by the thermal post-treatment. Because we expect functional groups to desorb as CO

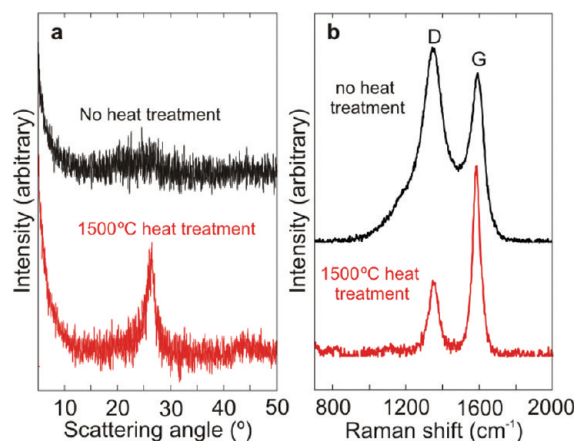


Figure 2. Structure of FGS₁₃ before and after 1500 °C heat treatment: (a) XRD profiles and (b) Raman shift.

or CO₂, such a reduction without annealing³⁹ increases the defect density of the FGSs by producing vacancies in the lattice.¹ However, the decrease in surface area and the emergence of a d_{0002} reflection in the XRD profile suggests that the heat treatment at 1500 °C is also sufficient to anneal the FGSs into small graphitic domains that likely form at overlapping regions. These claims are further substantiated by comparing the Raman spectra for FGS₁₃ before and after heat treatment (Figure 3b). The ratio of the intensities of the D band to the G band (I_D/I_G) decreased from 1.1 to 0.4 after the 1500 °C treatment. This ratio is related to the number of defects in the carbon lattice⁴⁰ and the observed decrease in I_D/I_G after heat treatment demonstrates that the defect density was reduced with respect to FGS₁₃. A recent transmission electron microscope (TEM) and Raman study on graphene nanoribbons heated to 1500 °C has also demonstrated that lattice defects begin to anneal out at this temperature.⁴¹ Annealing at higher temperatures (>2000 °C) is known to be necessary for nearly complete removal of the defects.⁴² Therefore, FGS₁₃ was also annealed using a higher temperature treatment (2250 °C). However, this material could no longer be dispersed as individual sheets, likely because the extent of graphitization between FGSs within the powder was so extreme that the ultrasonication procedure could no longer provide enough energy to separate the graphene sheets. Although we may not have removed all defects at 1500 °C, we will show that this material has a capacitance–potential (C/E) behavior that is similar to pristine graphene or HOPG.

Morphological Characterization of LB Films Transferred to Gold and HOPG. The secondary electron contrast of the SEM images of Figure 3 between the gold (bright) and LB film (dark) indicates that the film is composed of a monolayer of discretely tiled but densely packed FGSs. Although the exposed gold or underlying HOPG could be completely covered with FGSs, either by increasing the surface pressure or by applying multiple coatings, this inherently caused the formation of multilayers or overlapped regions between FGSs. The overlapping of sheets was avoided to prevent the formation of pores and related uncertainties in the accessible surface area of the FGS electrode. For FGS₂, a densely packed but discretely tiled coating was obtained at a surface pressure of 8 mN/m, whereas FGS₁₃ and FGS₃₈₅ required 20 and 30 mN/m, respectively. For FGS₁₃, a relative area coverage of $A_{rel} = 84\%$ with a standard deviation of only 3% was obtained, confirming a large degree of film homogeneity.

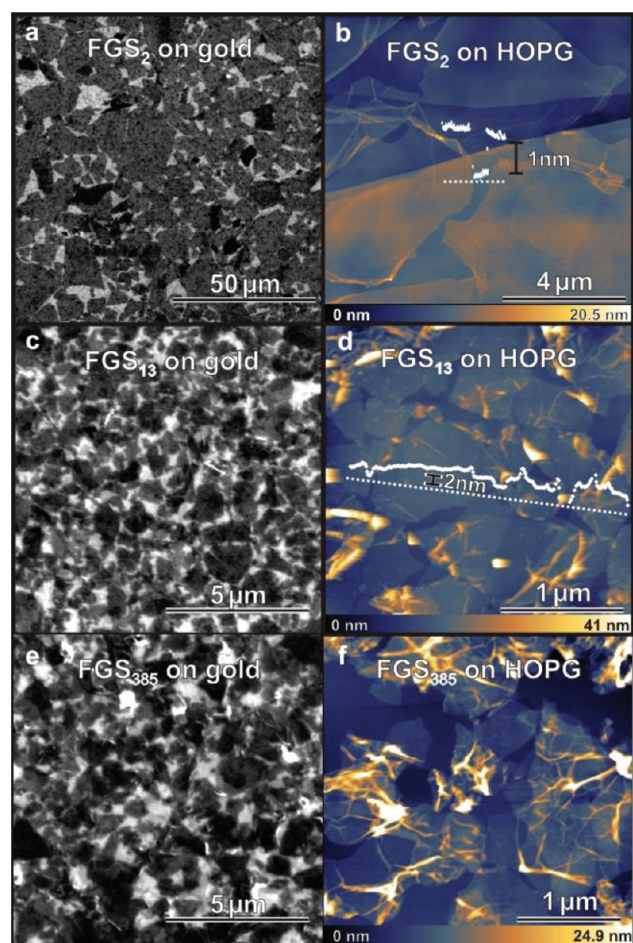


Figure 3. Morphology of FGSs on gold and HOPG substrates. (a) SEM image of FGS₂ coated on gold and tapping-mode. (b) AFM image of FGS₂ on HOPG. (c) SEM image of FGS₁₃ on gold and tapping-mode. (d) AFM image of FGS₁₃ on HOPG. (e) SEM images of FGS₃₈₅ on gold and tapping-mode. (f) AFM images of FGS₃₈₅ on HOPG.

The AFM images in Figure 3b,d,f demonstrate that the sheets conform to the topographical features of the substrates (e.g., edge-plane steps of the HOPG) and show wrinkles and folds. FGS₂ exhibits a thickness of ~1 nm and diameters of several tens of micrometers, as shown in Figure 3b. FGS₁₃ has a typical thickness of ~2 nm and a diameter of 1 μm or less, as shown in Figure 3d. The distribution of sheet thickness was similar to our previous studies and indicates that the FGS₁₃ system consists of a mixture of single and few-layer FGSs (Supporting Information, Figure S1). We attribute the increased thickness of FGS₁₃ compared with FGS₂ to functional groups and defects, as discussed by Schniepp et al.¹ As shown in Figure 3f, FGS₃₈₅ appears much more wrinkled than FGS₁₃. A thickness distribution for FGS₃₈₅ was not generated because the wrinkled nature of many of the sheets prohibited a reliable height measurement. However, the FGS₃₈₅ typically appeared thicker than FGS₁₃. We expect the thickness of an FGS to decrease as functional groups and lattice defects are removed. The appearance of thicker sheets with a higher degree of wrinkling is likely due to the formation of graphitic domains between adjacent sheets during the 1500 °C treatment, as evidenced by the appearance of a d_{0002} reflection in the XRD profiles (Figure 2a) and indicates that FGS₃₈₅ may be composed of a larger proportion of few-layer FGSs. Because in

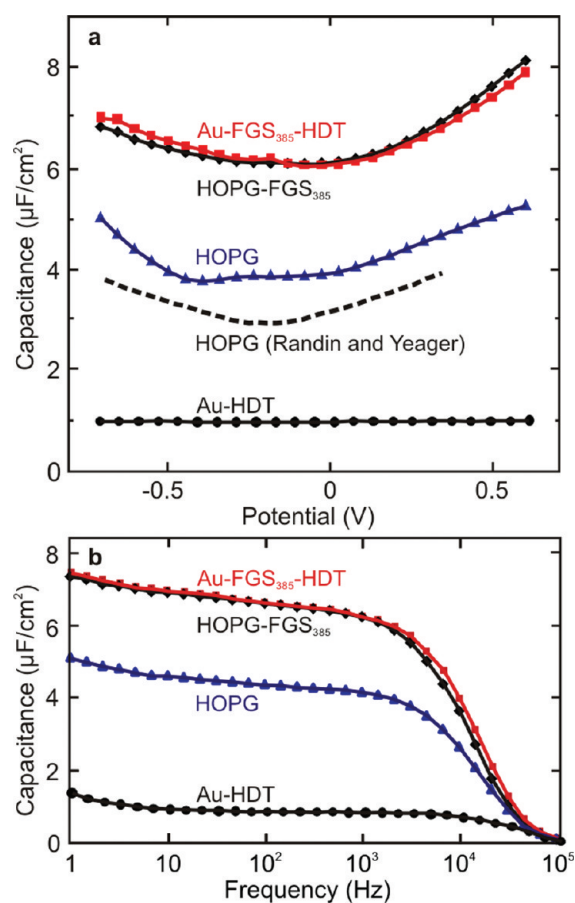


Figure 4. Capacitance of FGS₃₈₅ monolayers on gold and HOPG. (a) *C/E* curves of various electrodes in 0.5 M NaF measured at 1000 Hz. (b) Frequency dependence of the capacitance of various electrodes measured in 0.5 M NaF.

this study we are interested in the surface specific capacitance and not the mass specific capacitance, the presence of a population of multistacked sheets will not significantly affect our measurements.

Capacitance and Redox Activity of Reduced and Annealed FGS Monolayers. We first focus on the capacitance and redox activity of FGS₃₈₅ monolayers because we expect their electrochemical properties to be similar to what is observed with pristine graphene²⁷ and HOPG.²⁶ As shown in Figure 4a, the capacitance of the HOPG-FGS₃₈₅ electrode ranged from 7 to 9 μF/cm² between -0.7 and 0.6 V. The *C/E* curve has a smoothed V-shape with a small local maximum at -0.23 V and which was similar to what was reported by Randin and Yeager for a high-quality single-crystal (X-ray rocking angle <0.4°) HOPG surface with few edge-plane defects.²⁶ However, their curve does not show a local maximum, and we find that measurements made on a lower quality HOPG (8° rocking angle) that exhibited a larger density of edge-plane defects resemble our result more closely. The capacitance is fairly constant with frequency changing less than 10% between 10 and 1000 Hz (Figure 4b). Figure 4a also shows the capacitance measured for the underlying bare HOPG electrode. The shape of the *C/E* curve is similar to that for the HOPG-FGS₃₈₅ electrode but ranges between 4 and 6 μF/cm² and also displays a small local maximum near -0.23 V. The frequency dispersion of the capacitance was nearly identical to HOPG-FGS₃₈₅ (Figure 4b). Because frequency dispersion is associated

with surface roughness⁴³ or frequency-dependent Faradaic charging events,⁴⁴ the similar behavior between the atomically smooth, bare HOPG surface and HOPG-FGS₃₈₅ suggests that the FGS₃₈₅ monolayer coating introduces negligible surface roughness or porosity. The small but finite frequency dispersion for HOPG is likely associated with a high density of exposed edge-plane sites that may lead to the small local maximum observed at -0.23 V. AFM measurements indicated that edge-plane steps in our HOPG can be found every few micrometers. The edges and residual lattice defects within the FGS₃₈₅ monolayers may also contribute to a larger capacitance of FGS₃₈₅ compared with the HOPG. Because AFM images (Figure 3) indicate that many of the FGS₃₈₅ are wrinkled, it is also possible that some of the electrolyte penetrates beneath the wrinkled regions. This extra surface area could contribute to a higher measured capacitance compared with HOPG.

To ensure that the underlying HOPG electrode does not significantly influence the measured capacitance of the FGS₃₈₅ monolayers, we also tested the capacitance of FGS₃₈₅ monolayers on gold. Because the capacitance of gold is known to be much larger than HOPG (Supporting Information, Figure S2), the exposed gold was passivated with HDT prior to measuring the capacitance of the FGS₃₈₅ monolayers. Figure 4a shows the capacitance of Au-FGS₃₈₅-HDT. The *C/E* curve is found to lie nearly on top of the HOPG-FGS₃₈₅ curve, and the frequency dispersion (Figure 4b) is also nearly identical. The Au-HDT response, in the absence of FGS₃₈₅, is also shown in Figure 4. The capacitance is constant (~1 μF/cm²) within the potential limits and shows a frequency dispersion similar to that observed for HOPG and HOPG-FGS₃₈₅. Because the Au-FGS₃₈₅-HDT monolayer shows no evidence of the underlying gold capacitance and the shape of the Au-HDT capacitance is nearly constant with potential, we conclude that we are indeed measuring the capacitance of the FGS₃₈₅ monolayer only. The similarity between the behavior on HOPG and passivated gold also demonstrates that the thiol coating process has no measurable effect on the electrochemical behavior of the FGS₃₈₅ monolayers.

The redox activity of monolayer-coated electrodes was determined by recording cyclic voltammograms (CVs) in 5 mM potassium ferrocyanide solution, as shown in Figure 5. In the case of potassium ferrocyanide in an inert supporting electrolyte, the separation between oxidation and reduction peaks (E_{pp}) is an indicator of whether the charge transfer reaction is limited by diffusion or by the kinetics of heterogeneous charge transfer across the electrode/electrolyte interface.⁴⁵ CVs for FGS₃₈₅ on HOPG and gold at a scan rate of 100 mV/s are shown in Figure 5a. Both electrodes are capable of oxidizing and reducing the redox couple, and the CVs lie nearly on top of one another. Figure 5b shows that between 20 and 2000 mV/s E_{pp} depends only weakly on the scan rate, which is indicative of a solely diffusion limited reaction.⁴⁵ The small increase in E_{pp} with scan rate is likely due to uncompensated solution resistance, although kinetic limitations cannot be fully excluded.

Conversely, electron transfer across a pristine HOPG electrode/electrolyte interface is slow; therefore, CVs exhibit characteristics of a kinetically limited rather than diffusion-limited reaction.²⁹ Figure 5b shows a strong dependence of E_{pp} with scan rate when bare HOPG electrodes are used. However, this behavior was only observed during the first few uses of an HOPG block. After several experiments with the same HOPG block (involving repeated peeling of the HOPG), the reaction at the electrode surface became diffusion-limited, as indicated by a

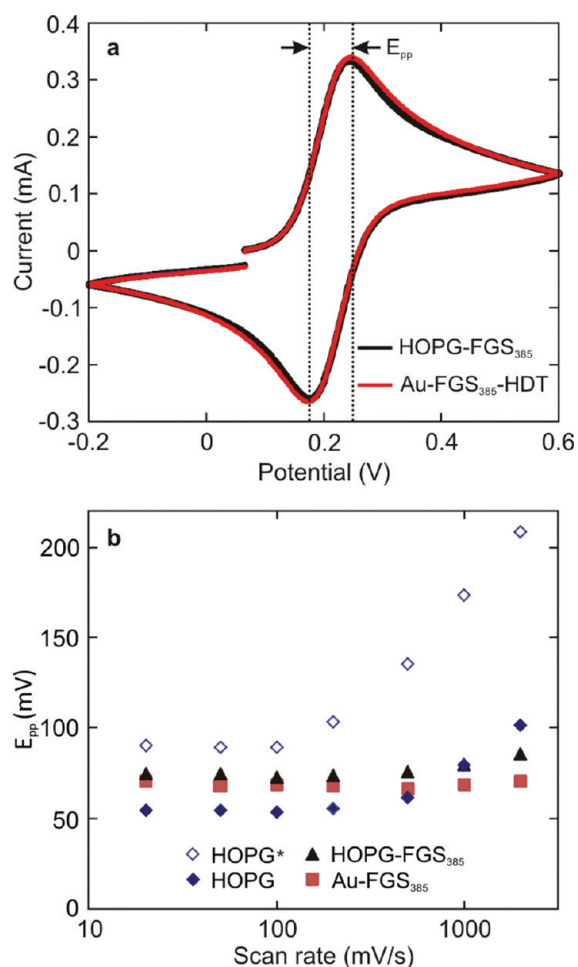


Figure 5. Redox response of FGS₃₈₅ monolayers analyzed by cyclic voltammetry. (a) CVs of monolayer electrodes carried out in 5 mM potassium ferrocyanide in 0.5 M NaF carried out at 100 mV/s. (b) Dependence of E_{pp} on scan rate for various electrodes. (*HOPG used had only been cleaved once before.)

nearly constant E_{pp} near the theoretical value of 56 mV. After repeated use, the HOPG developed edge-plane defects every few micrometers. These edge-plane defects are known to display anomalously fast kinetics, and their close spacing caused the electrode to behave as an array of closely spaced microelectrodes leading to a diffusion-limited reaction.²⁹ Although the basal plane of the FGS₃₈₅ is also expected to show kinetic limitations, the presence of closely spaced edges may also lead to the observed diffusion limitations for FGS₃₈₅ monolayers.

Capacity and Redox Activity of FGS₂. Now that we have demonstrated our ability to isolate the electrochemical properties of FGS₃₈₅ monolayers, which showed a similar capacitance behavior to HOPG or pristine graphene, we analyze the most highly oxidized form of graphene, FGS₂. Because FGS₂ is known to be an electrical insulator, we expected that monolayers of FGS₂ would at least partially block the electrochemical behavior of the underlying HOPG or gold electrodes. When FGS₂ monolayers are present on the HOPG surface, the CVs obtained with the redox probe change considerably (see Figure 6a). At 100 mV/s, E_{pp} increased from 56 to >500 mV, which indicates that the FGS₂ film is indeed insulating and blocks many of the electroactive edge-plane sites on the bare HOPG surface. Figure 6b shows that the presence of the FGS₂ monolayer decreases

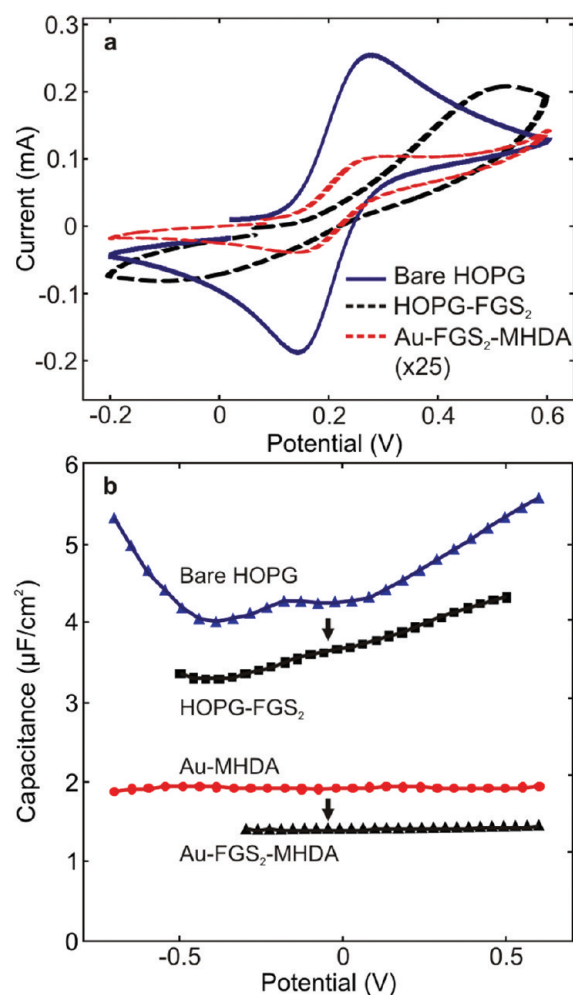


Figure 6. Electrochemical behavior of gold- and HOPG-coated FGS₂ monolayers. (a) CVs in 5 mM potassium ferrocyanide and 0.5 M NaF measured at 100 mV/s compared with bare gold. (b) C/E curves of various electrodes in 0.5 M NaF measured at 100 Hz.

the capacitance by $\sim 1 \mu\text{F}/\text{cm}^2$. (The applied potential was kept above -0.5 V to prevent electrochemical reduction of the FGS₂.) Because FGS₂ is a dielectric, a decrease in the capacitance is expected: Its presence increases the distance between the electrically conducting electrode and ionic species in solution.

When the HDT coating was applied to Au-FGS₂ electrodes, FGS₂ were found to roll and crumple, forming a sparse needle-like morphology on the gold surface (Supporting Information, Figure S3). This problem was ameliorated by using a hydrophilic MHDA coating that allowed the sheets to retain their densely tiled, flat conformation. Figure 6a shows that the oxidation peak current for the redox probe at a Au-FGS₂-MHDA electrode was reduced by a factor of >50 with respect to bare gold and was similar to the response of gold passivated with only MHDA. The capacitance of Au-MHDA and Au-FGS₂-MHDA is shown in Figure 6b. The FGS₂ coating decreases the capacitance by $\sim 0.5 \mu\text{F}/\text{cm}^2$. As with the HOPG-FGS₂ electrodes, these results indicate that FGS₂ is not electroactive but acts as a blocking layer.

Capacity and Redox Activity of FGS₁₃ and Electrochemically Reduced FGSs. We now investigate the electrochemical behavior of FGSs that are electrically conducting but have not been annealed at high temperatures and thus contain a larger number of lattice

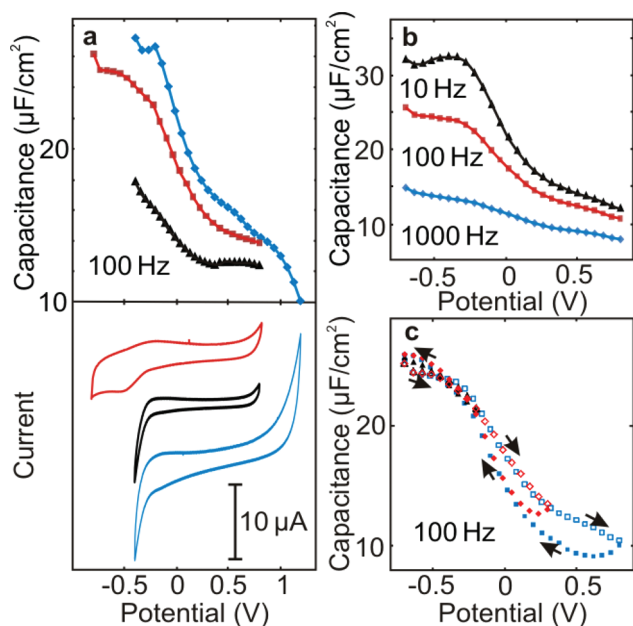


Figure 7. Electrochemical characterization of FGS₁₃ monolayers. (a) *C/E* dependence on the potential history for HOPG-FGS₁₃ in 0.5 M NaF (top) measured after cycling 10 times between the minimum and maximum potential limits carried out in the CVs (bottom). All measurements were made on the same sample starting with the -0.4 to 0.7 V range then moving from -0.9 to 0.7 V and finally from -0.4 to 1.2 V. (b) *C/E* curves for HOPG-FGS₁₃ in 0.5 M NaF at various frequencies. (c) Hysteresis of *C/E* with respect to whether the capacitance was measured from negative to positive potentials or positive to negative potentials.

defects and functional groups compared with FGS₃₈₅. We first contrast the behavior of FGS₃₈₅ with FGS₁₃, the material obtained by the rapid thermal expansion of GO without any thermal post treatment. Figure 7a shows the *C/E* behavior of HOPG-FGS₁₃ and the corresponding CVs within three different potential windows in the range between -0.8 and 1.2 V. Over all potential limits explored, the capacitance is significantly larger compared with our observations with FGS₃₈₅ and increases further as the potential window is expanded. This increase in capacitance is irreversible because the *C/E* curves obtained within the intermediate potential window cannot be reproduced after the electrodes have been subjected to more extreme potentials. CVs recorded in the supporting electrolyte are symmetric and indicative of double-layer charging with the capacitive charging current also increasing as the potential window is made larger. The small peak observed at -0.5 V decreased in magnitude with inert gas purging and is attributed to the reduction of residual oxygen in the electrolyte.

The capacitance of the FGS₁₃ electrode depends largely on the measurement frequency (Figure 7b) and shows hysteresis upon reversal of the direction of the potential scan (Figure 7c). This is indicative of Faradaic charging and is typically observed also at other carbonaceous electrodes such as glassy carbon and edge-plane HOPG: Surface functional groups on these materials cause a charging behavior that changes depending on frequency, electrolyte pH, potential range, and scan direction. Randin and Yeager have shown that the capacitance of such surfaces ranges from 10 to $70 \mu\text{F}/\text{cm}^2$.^{21,26} Our results lie within this range and suggest that FGS₁₃ prior to annealing behaves more like glassy

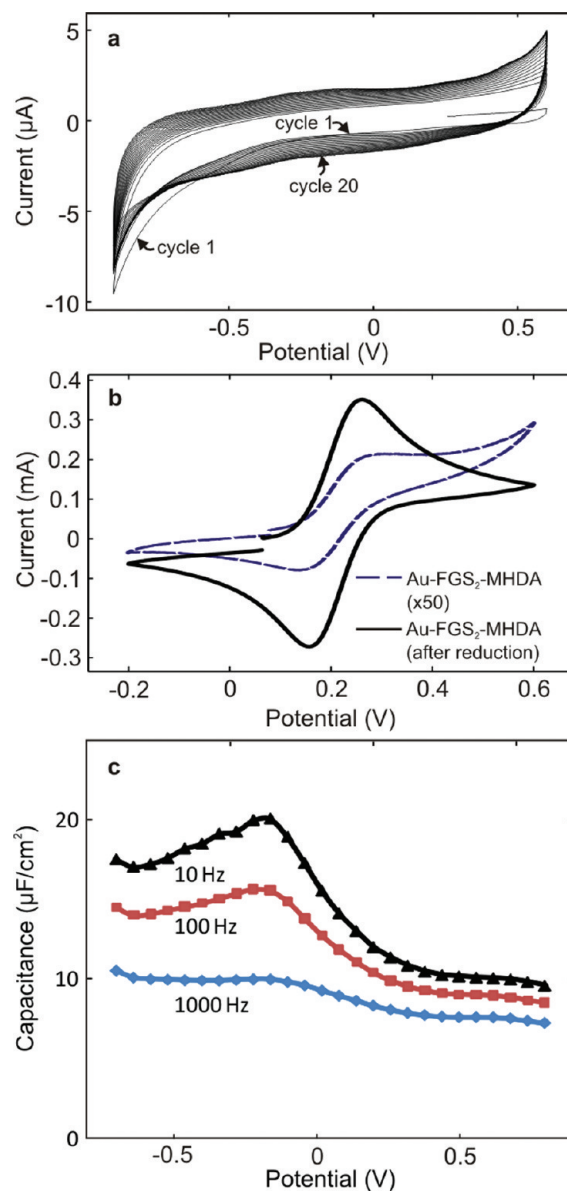


Figure 8. Characterization and electrochemical reduction of FGS₂ on gold. (a) CVs of Au-FGS₂-MHDA used to electrochemically reduce FGS₂ in 0.5 M NaF supporting electrolyte at 100 mV/s. (b) CVs in 5 mM potassium ferrocyanide and 0.5 M NaF before and after electrochemical reduction. (c) *C/E* curves of Au-FGS₂-MHDA after electrochemical reduction measured at various frequencies.

carbon or the edge-plane of HOPG rather than the basal-plane of HOPG. Our results for Au-FGS₁₃-HDT were confirmed by measurements with FGS₁₃ monolayers on HOPG (Supporting Information, Figure S4).

The FGS₁₃ monolayers were also redox-active and displayed the same diffusion-limited redox behavior as FGS₃₈₅ (see Supporting Information, Figure S5). We expect the basal-plane of FGS₁₃ to facilitate electron transport because compared with FGS₃₈₅ it is more defective and decorated with functional groups, but we currently cannot distinguish between the reactivity of electroactive edge-plane sites and the basal-plane using cyclic voltammetry in this system.

Besides starting with monolayers of FGSs reduced/annealed in bulk, our system is also capable of measuring FGSs produced

Table 1. Summary of the Physical and Electrochemical Properties of Various FGSs^a

sample	C/O ratio	I_D/I_G ratio	min. capacitance ($\mu\text{F}/\text{cm}^2$)	max. capacitance ($\mu\text{F}/\text{cm}^2$)	E_{pp}
FGS ₂	2		3.3	4.3	627
FGS ₁₃	13	1.1	13.9	26.1	62
erFGS	24		8.5	15.6	102
FGS ₃₈₅	385	0.4	6.6	8.8	73
HOPG	∞	0.3	4.0	5.6	133

^aCapacitance is reported for 100 Hz and E_{pp} is reported for 100 mV/s using monolayers on HOPG. The C/O ratio of erFGS was not measured but taken from the literature.⁴⁸

by reducing monolayers of FGS₂ to an undefined C/O ratio. As an example, FGS₂ can be electrochemically reduced to electrically conducting FGSs (referred to as erFGS).^{46,47} Using our monolayer system, we performed such a reduction and subsequently determined the impact on the electrochemical properties of the resulting FGSs. The electrochemical reduction of FGS₂ monolayers was carried out by cycling the Au-FGS₂-MHDA electrodes repeatedly to -0.9 V. As shown in Figure 8a, the capacitive charging current increased with cycling and equilibrated after ~ 20 cycles. This indicated that the FGS₂ monolayers were reduced to conducting erFGS. The electrodes were then further characterized with the ferrocyanide redox probe and by EIS to determine their capacitance.

As shown in Figure 8b, monolayers of erFGS are capable of oxidation and reduction of the ferro/ferricyanide redox couple. The capacitance of the electrode (Figure 8c) lies between 8 and 14 $\mu\text{F}/\text{cm}^2$ depending on the electrode potential and thus is significantly smaller than the capacitance of FGS₁₃ monolayers. The shape of the C/E curve is similar to that of FGS₁₃ but exhibits a smaller asymmetry between negative and positive potentials. There are no indications of exposed gold in the CVs or the C/E data, confirming that the thiol coating remains stable during the electrochemical reduction of FGS₂.

FGS₁₃ and erFGS can be expected to exhibit different atomic structure and composition that may result in different electrochemical properties.⁴ The number and type of functional groups after electrochemical reduction compared with rapid thermal reduction may be different. It has, for example, been shown that the C/O ratio of erFGS reduced at a similar potential as used by us was 24.⁴⁸ A smaller density of functional groups may lead to less pseudocapacitance, which might explain the difference we observe between erFGS (8–14 $\mu\text{F}/\text{cm}^2$) and FGS₁₃ (15–35 $\mu\text{F}/\text{cm}^2$). Also, a comparably large number of lattice defects may be introduced during thermal reduction of GO, which may lead to increases in capacitance. Furthermore, the FGS₁₃ used in this study are typically smaller in diameter (~ 1 μm) compared with erFGS (~ 10 μm). Therefore, a larger number of edge-plane sites exist for FGS₁₃. Because the edge-plane of graphite is known to exhibit a larger capacitance than the basal-plane,²¹ the smaller diameter of FGS₁₃ may contribute to the observed capacitance of the material.

Monolayers of FGS₂ can be reduced not only by electrochemical methods but also by using our system together with other techniques such as chemical (hydrazine, sodium borohydride)¹³ and thermal^{1,2} reduction and to study and systematically compare their impact on the electrochemical properties of the resulting FGSs.

A comparison of the properties of the various types of FGSs used in this study is given in Table 1. The capacitance tends to increase with decreasing C/O ratio (down to 13). Also, the capacitance increases with increasing I_D/I_G ratio, suggesting that the defect density could be increasing the capacitance of the material. However, it is currently unknown whether this capacitance increase is due to pseudocapacitive (i.e., faradaic) contributions or due to changes in C_{dl} of the FGS/electrolyte interface. We are currently working on extending our work to the use of nonaqueous electrolytes where pseudocapacitance is suppressed and a direct comparison of C_{dl} of various types of FGSs can be made, and its dependence on both functional groups and defects can be explored.

4. CONCLUSIONS

Using densely tiled monolayers of FGSs on passivated gold and HOPG, we have developed an electrode system with which we can isolate the electrochemical properties of various types of FGSs. Our method allows for the systematic study of different production and processing conditions for graphene materials and is not affected by artifacts induced through uncertainties in electrode porosity and accessible surface area. We demonstrated the capabilities of our system to perform measurements on FGS monolayers prepared either by the thermal expansion and reduction of GO (resulting in a carbon to oxygen (C/O) ratio of 13 and 385) or by reducing graphene oxide (C/O ratio ~ 2) electrochemically directly on the substrate. Instead of contacting a single graphene sheet and measuring mostly the properties of only the basal-plane, we analyze the response of ensembles of single sheets including both the basal-plane and edge-plane contributions. Our method therefore allows for the prediction of the electrochemical properties of bulk graphene electrodes.

We found that graphene oxide, because of the fact that it is electrically insulating, exhibits a blocking effect on the redox activity and lowers the capacitance of the underlying electrode. FGSs with a C/O ratio of 13 produced by the thermal exfoliation of GO, were found to have a large capacitance of up to 32 $\mu\text{F}/\text{cm}^2$ that depended on frequency and on the explored potential range, indicating a possible contribution from pseudocapacitance. A similar behavior was observed for erFGS. However, the capacitance of erFGS was significantly smaller than the capacitance of FGS₁₃. When FGS₁₃ was annealed at 1500 °C, its capacitance was shown to approach that of HOPG and pristine graphene.

This study demonstrates that the electrochemical properties of FGSs depend strongly on the reduction and annealing conditions used. The use of FGS monolayer electrodes to study FGSs will be critical for understanding how the composition and structure of FGSs affect important electrochemical properties like the intrinsic double-layer capacitance.

■ ASSOCIATED CONTENT

S Supporting Information. Further information on morphological and electrochemical characterization of FGS monolayer electrodes. This material is available free of charge via the Internet at <http://pubs.acs.org>.

■ AUTHOR INFORMATION

Corresponding Author

*E-mail: iaksay@princeton.edu.

ACKNOWLEDGMENT

This work was supported by an Army Research Office (ARO)/Multidisciplinary Research Initiative (MURI) under grant number W911NF-09-1-0476 and the Pacific Northwest National Laboratory under grant number DE-AC05-76RL01830. C.P. acknowledges support by the Alexander von Humboldt Foundation.

REFERENCES

- (1) Schniepp, H. C.; Li, J. L.; McAllister, M. J.; Sai, H.; Herrera-Alonso, M.; Adamson, D. H.; Prud'homme, R. K.; Car, R.; Saville, D. A.; Aksay, I. A. *J. Phys. Chem. B* **2006**, *110*, 8535–8539.
- (2) McAllister, M. J.; Li, J. L.; Adamson, D. H.; Schniepp, H. C.; Abdala, A. A.; Liu, J.; Herrera-Alonso, M.; Milius, D. L.; Car, R.; Prud'homme, R. K.; Aksay, I. A. *Chem. Mater.* **2007**, *19*, 4396–4404.
- (3) Pumera, M. *Energy Environ. Sci.* **2011**, *4*, 668–674.
- (4) Pumera, M. *Chem. Soc. Rev.* **2010**, *39*, 4146–4157.
- (5) Chen, D.; Tang, L.; Li, J. *Chem. Soc. Rev.* **2010**, *39*, 3157–3180.
- (6) Shao, Y. Y.; Wang, J.; Wu, H.; Liu, J.; Aksay, I. A.; Lin, Y. H. *Electroanalysis* **2010**, *22*, 1027–1036.
- (7) Pumera, M. *Chem. Rec.* **2009**, *9*, 211–223.
- (8) Punckt, C.; Pope, M. A.; Liu, J.; Lin, Y. H.; Aksay, I. A. *Electroanalysis* **2010**, *22*, 2834–2841.
- (9) Stankovich, S.; Dikin, D. A.; Piner, R. D.; Kohlhaas, K. A.; Kleinhammes, A.; Jia, Y.; Wu, Y.; Nguyen, S. T.; Ruoff, R. S. *Carbon* **2007**, *45*, 1558–1565.
- (10) Dai, X.; Wildgoose, G. G.; Compton, R. G. *Analyst* **2006**, *131*, 901–906.
- (11) Stuart, E. J. E.; Pumera, M. *J. Phys. Chem. C* **2010**, *114*, 21296–21298.
- (12) Yang, D.; Velamakanni, A.; Bozoklu, G.; Park, S.; Stoller, M.; Piner, R. D.; Stankovich, S.; Jung, I.; Field, D. A.; Ventrone, C. A.; Ruoff, R. S. *Carbon* **2009**, *47*, 145–152.
- (13) Dreyer, D. R.; Park, S.; Bielawski, C. W.; Ruoff, R. S. *Chem. Soc. Rev.* **2010**, *39*, 228–240.
- (14) Korkut, S.; Ozbaz, B.; Milius, D. L.; Liu, J.; Aksay, I. A. *Chem. Mater.* **2011**, submitted.
- (15) Roy-Mayhew, J. D.; Bozym, D. J.; Punckt, C.; Aksay, I. A. *ACS Nano* **2010**, *4*, 6203–6211.
- (16) Menshykau, D.; Compton, R. G. *Electroanalysis* **2008**, *20*, 2387–2394.
- (17) Si, Y. C.; Samulski, E. T. *Chem. Mater.* **2008**, *20*, 6792–6797.
- (18) Stoller, M. D.; Park, S. J.; Zhu, Y. W.; An, J. H.; Ruoff, R. S. *Nano Lett.* **2008**, *8*, 3498–3502.
- (19) Hantel, M. M.; Kaspar, T.; Nesper, R.; Wokaun, A.; Kötz, R. *Electrochem. Commun.* **2011**, *13*, 90–92.
- (20) Goh, M. S.; Pumera, M. *Electrochem. Commun.* **2010**, *12*, 1375–1377.
- (21) Randin, J. P.; Yeager, E. J. *Electroanal. Chem.* **1975**, *58*, 313–322.
- (22) Brownson, D. A. C.; Banks, C. E. *Chem. Commun.* **2012**, in press.
- (23) Qu, D. Y.; Shi, H. J. *Power Sources* **1998**, *74*, 99–107.
- (24) Chmiola, J.; Yushin, G.; Gogotsi, Y.; Portet, C.; Simon, P.; Taberna, P. L. *Science* **2006**, *313*, 1760–1763.
- (25) Pelskov, Y. V.; Sakharova, A. Y.; Krotova, M. D.; Bouilov, L. L.; Spitsyn, B. V. *J. Electroanal. Chem.* **1987**, *228*, 19–27.
- (26) Randin, J. P.; Yeager, E. J. *Electroanal. Chem.* **1972**, *36*, 257–276.
- (27) Xia, J. L.; Chen, F.; Li, J. H.; Tao, N. J. *Nat. Nanotechnol.* **2009**, *4*, 505–509.
- (28) Li, W.; Tan, C.; Lowe, M. A.; Abruña, H. C. D.; Ralph, D. C. *ACS Nano* **2011**, *5*, 2264–2270.
- (29) Davies, T. J.; Hyde, M. E.; Compton, R. G. *Angew. Chem., Int. Ed.* **2005**, *44*, 5121–5126.
- (30) Cote, L. J.; Kim, F.; Huang, J. X. *J. Am. Chem. Soc.* **2009**, *131*, 1043–1049.
- (31) Li, X. L.; Zhang, G. Y.; Bai, X. D.; Sun, X. M.; Wang, X. R.; Wang, E.; Dai, H. J. *Nat. Nanotechnol.* **2008**, *3*, 538–542.
- (32) Hummers, W. S.; Offeman, R. E. *J. Am. Chem. Soc.* **1958**, *80*, 1339–1339.
- (33) Kim, J.; Cote, L. J.; Kim, F.; Yuan, W.; Shull, K. R.; Huang, J. X. *J. Am. Chem. Soc.* **2010**, *132*, 8180–8186.
- (34) Brunauer, S.; Emmett, P. H.; Teller, E. *J. Am. Chem. Soc.* **1938**, *60*, 309–319.
- (35) Zhavnerko, G. K.; Agabekov, V. E.; Yaminsky, I. V. Formation of Langmuir Monolayers For AFM Studies By the “Horizontal Precipitation” Method. In *Physics, Chemistry and Application of Nanostructures: Reviews and Short Notes to Nanomeeting '99*; Borisenko, V. E., Gaponenko, S. V., Gurin, V. S., Eds.; World Scientific: Singapore, 1999; pp 218–220.
- (36) Bowler, R.; Davies, T. J.; Hyde, M. E.; Compton, R. G. *Anal. Chem.* **2005**, *77*, 1916–1919.
- (37) Schniepp, H. C.; Shum, H. C.; Saville, D. A.; Aksay, I. A. *J. Phys. Chem. C* **2008**, *112*, 14902–14906.
- (38) Hamelin, A. J. *Electroanal. Chem.* **1996**, *407*, 1–11.
- (39) Sato, K.; Saito, R.; Oyama, Y.; Jiang, J.; Cañado, L. G.; Pimenta, M. A.; Jorio, A.; Samsonidze, G. G.; Dresselhaus, G.; Dresselhaus, M. S. *Chem. Phys. Lett.* **2006**, *427*, 117–121.
- (40) Dresselhaus, M. S.; Jorio, A.; Hofmann, M.; Dresselhaus, G.; Saito, R. *Nano Lett.* **2010**, *10*, 751–758.
- (41) Campos-Delgado, J.; Kim, Y. A.; Hayashi, T.; Morelos-Gómez, A.; Hofmann, M.; Muramatsu, H.; Endo, M.; Terrones, H.; Shull, R. D.; Dresselhaus, M. S.; Terrones, M. *Chem. Phys. Lett.* **2009**, *469*, 177–182.
- (42) Platonov, P. A.; Trofimchuk, E. I.; Chugunov, O. K.; Karpukhin, V. I.; Tumanov, Y. P.; Alexeev, S. I. *Radiat. Eff.* **1975**, *25*, 105–110.
- (43) Scheider, W. J. *Phys. Chem.* **1975**, *79*, 127–136.
- (44) Conway, B. E. *Electrochemical Supercapacitors: Scientific Fundamentals and Technological Applications*; Kluwer Academic: New York, 1999.
- (45) Nicholson, R. S.; Shain, I. *Anal. Chem.* **1964**, *36*, 706–723.
- (46) Wang, Z. J.; Zhou, X. Z.; Zhang, J.; Boey, F.; Zhang, H. J. *Phys. Chem. C* **2009**, *113*, 14071–14075.
- (47) Shao, Y. Y.; Wang, J.; Engelhard, M.; Wang, C. M.; Lin, Y. H. *J. Mater. Chem.* **2011**, *20*, 743–748.
- (48) Zhou, M.; Wang, Y. L.; Zhai, Y. M.; Zhai, J. F.; Ren, W.; Wang, F. A.; Dong, S. J. *Chem.—Eur. J.* **2009**, *15*, 6116–6120.